Journal of Paleontology, 93(3), 2019, p. 476–495
Copyright © 2019, The Paleontological Society
0022-3360/19/1937-2337
doi: 10.1017/jpa.2018.96

JOURNAL OF PALEONTOLOGY
A PUBLICATION OF THE Paleontological SOCIETY

Frasnian-Famennian transition in western Thailand: conodonts, biofacies, eustatic changes, extinction

Norman M. Savage

Department of Earth Sciences, University of Oregon, Eugene, OR 97403, USA <nmsavage@uoregon.edu>

Abstract.—The biofacies of the Lower *Palmatolepis rhenana* Biozone to *Palmatolepis triangularis* Biozone in the Mae Sariang section, northwestern Thailand, are marked by alternations of *Palmatolepis*-dominated biofacies and *Polygnathus*-dominated biofacies related to fluctuations in seawater depth. Fine-grained limestone accumulated through the Lower *Palmatolepis rhenana* Biozone, Upper *Palmatolepis rhenana* Biozone, *Palmatolepis linguiformis* Biozone, *Palmatolepis subperlobata* Biozone, and *Palmatolepis triangularis* Biozone. A regression in the Upper *rhenana* Zone was followed by a recovery transgression that extended up through the *linguiformis* Zone. Conodont faunas increased until near the end of the *linguiformis* Zone, but in the overlying *subperlobata* Zone and *triangularis* Zone, conodont numbers dropped and most conodont species disappeared. It is possible the event coincides with a glacially forced regression, but there is no evidence of this in the section apart from a positive spike in δ13C. Another possible cause of the global marine extinction event is toxic levels of metals resulting from widespread volcanism. New taxa in this paper are *Palmatolepis chaemensis* new species, *Palmatolepis thamensis* new species, and *Polygnathus tenellus surinensis* new subspecies.

UUID: http://zoobank.org/f2b55ba8-fe49-46f6-a2d5-bfd0208f1460

Introduction

Late Devonian conodonts of northwest Thailand have been described previously by several workers, including Wongwanich and Burrett (1984), Burrett et al. (1986), Savage et al. (2006), Königshof et al. (2012), and Savage (2013). This paper concentrates on a small but important Frasnian interval 80 cm thick that extends through the Upper *Palmatolepis rhenana* Biozone, the Lower *Palmatolepis rhenana* Biozone, the *Palmatolepis linguiformis* Biozone, the Frasnian-Famennian global extinction event, and into the beginning of the *Palmatolepis triangularis* Biozone. Some of the conodonts from the upper part of this interval were illustrated and described by Savage (2013) and are reillustrated herein because that booklet is not readily available.

Geologic setting

In Savage (2013), a near-vertical section 11 m thick near the town of Mae Sariang was described, and the conodont faunas and geochemistry were discussed. Although the cliff section is 11 m thick, a thrust fault repeats part of the section so that the Frasnian and Famennian thickness is 7.8 m. The locality is 20 km southwest of Mae Sariang at 18°01′07″N, 97°51′3″E (Fig. 1).

A steep, almost vertical cliff more than 20 m high is set back from the roadside and largely obscured by trees. The section was discovered by the author in 2006, in the company of A. Sardsud. At the time of our 2006 visit, the section had not been described and its importance was not appreciated, although we suspected it was largely of Devonian age.

To take preliminary samples for conodont analysis, our assistants climbed the cliff and numbered the beds with paint from D1 at the top down to D26 at the base. These numbers were used subsequently and are in reverse order of deposition. After these preliminary samples had been processed for conodonts, we returned in 2007. Following construction of a bamboo stairway up the cliff, we measured and marked the 18 Upper Devonian beds, D1 to D18, which were subdivided into 80 intervals, each about 11–15 cm thick (see Savage 2013, fig. 2). The interval thicknesses were not arbitrary but were determined by the thickness of the larger beds. From each of these 80 intervals, conodont samples of about 2 kg were collected and processed at the University of Oregon. The samples all yielded conodonts, varying from 10s per kilogram to over 1,000 elements per kilogram. The beds contain very few megafossils although some ostracode, crinoid, and trilobite fragments have been found in thin sections (Königshof et al., 2012). In related work, G. Racki and colleagues J. Dopieralska and Z. Belka began a comparison of neodymium isotopes at the Mae Sariang section and at another section farther south at Thong Pha Phum (Dopieralska et al., 2012).

Materials and methods

Most of the materials were collected by the author between 2006 and 2010, accompanied variously by Dr. A. Sardsud of the Department of Mineral Resourses, Dr. P. Lutat of Mahrasarakham University, and in 2009 and 2010 by Drs. Sarsud and Lutat together with Dr. P. Königshof of the Senkenberg Research Institute, Germany.

https://doi.org/10.1017/jpa.2018.96 Published online by Cambridge University Press

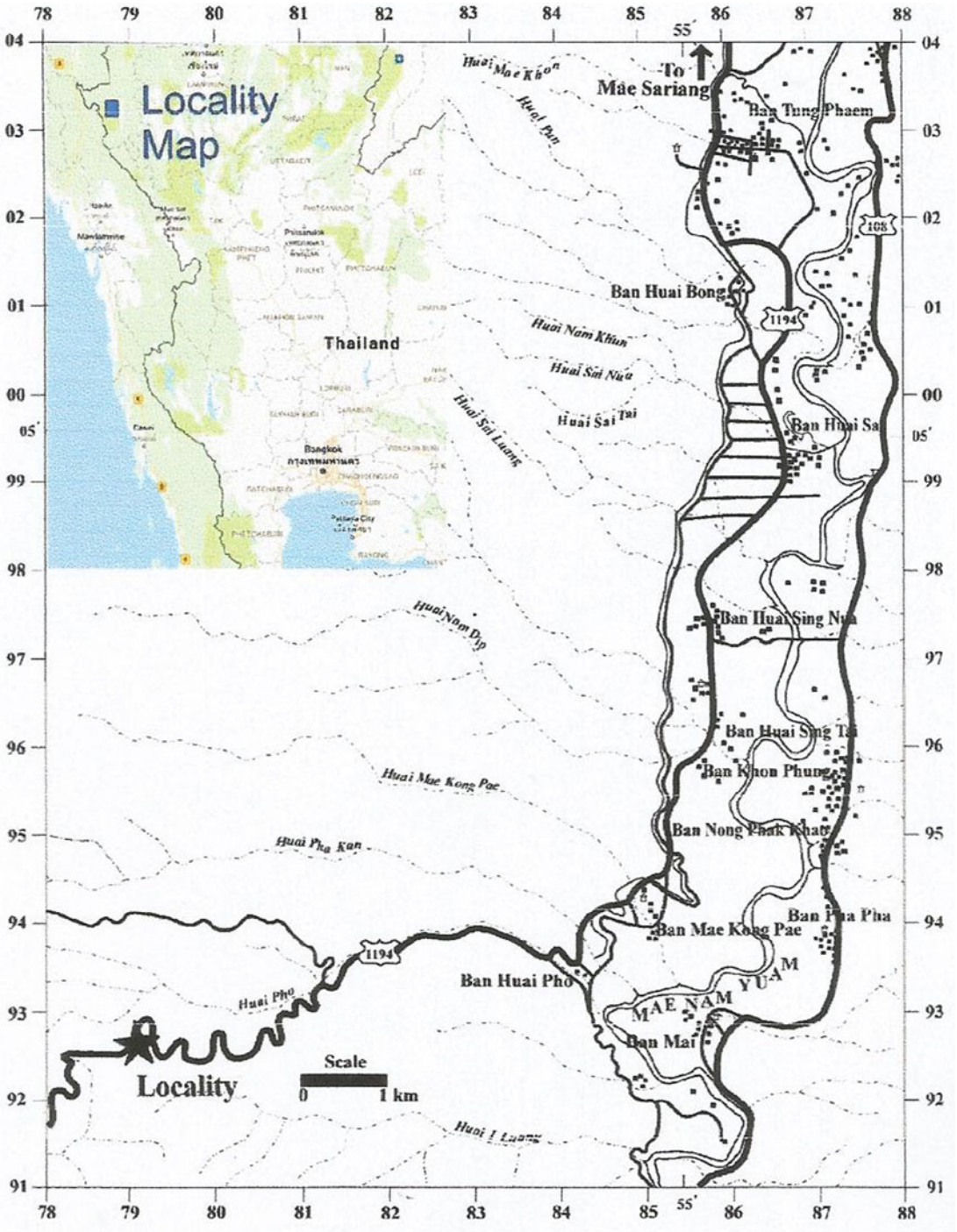


Figure 1. Location of the Mae Sariang section, 20 km southwest of Mae Sariang, northwestern Thailand, at 18°01′07″N, 97°51′30″E.

This Mae Sariang section is exposed where a stream is cutting into the cliff. During the wet season (July to October) the stream may become a waterfall, with most of the water passing through a conduit beneath the road. This erosion is a two-edged sword in that it keeps the exposure renewed but also causes large blocks to break away. A house-sized block broke from the central part of our exposure and fell down to the road in 2010 just before our field party arrived at the site (Fig. 2.1). This was a few meters east of our bamboo stairway, built three years earlier. Fortunately, the fall improved the exposure and allowed us to collect new samples from beds D17 and D18 a meter farther east from the earlier painted intervals (Fig. 2.2, 2.3, 2.5).

Herein the author concentrates on the part of the section that includes the Frasnian-Famennian extinction event and describes conodonts from the seven horizons D18-E up through D17-F (Fig. 3). Conodonts from most of these horizons at Mae Sariang have not been described earlier. Previously the author divided

https://doi.org/10.1017/jpa.2018.96 Published online by Cambridge University Press

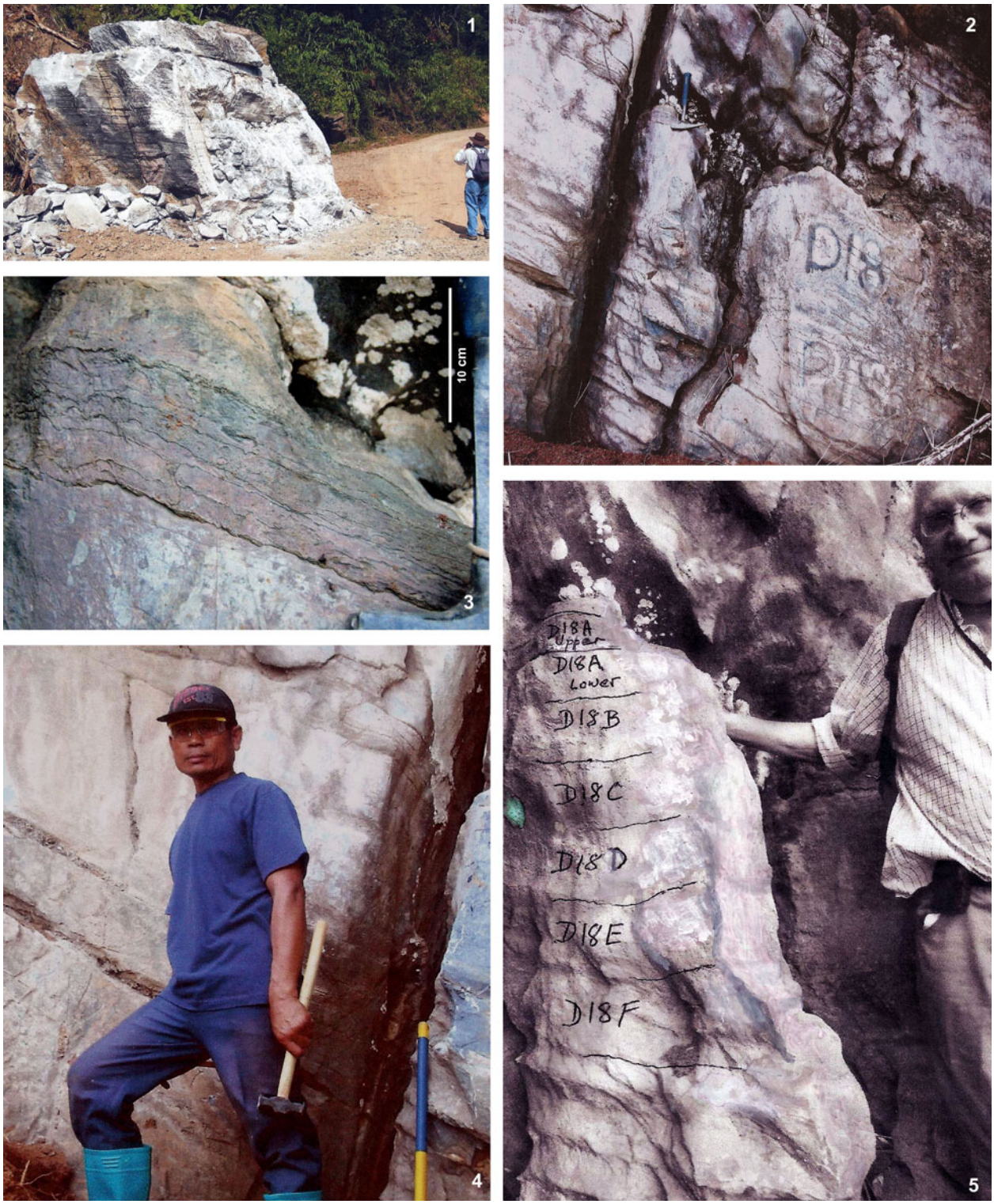


Figure 2. Photographs at the section. (**1**) Fallen block on the road below the section, November 2010; (**2**) horizons D17 (above), D18, and D19 (below), with hammer leaning against the brownish layers in upper part of D18 and D18AEx; (**3**) close-up of part of (**2**) to show the two brownish layers in upper part of D18, hammer for scale, also 10 cm scale bar; (**4**) field assistant standing in front of beds D18 and D19, at the left side of picture in image (**2**) with top of his cap level with the brownish layers that continue to his right; (**5**) photograph of part of D17, D18, and D19 (see Figure 2.2) with markings of where samples were taken in 2010.

the D18-A interval into lower and upper parts (Savage, 2013, p. 11, 13), but herein these are termed D18-A for the lower part of the *linguiformis* Zone and D18-AEx for the upper part of that zone.

Repository and institutional abbreviation.—Types and figured specimens in this study are in the Condon Collection, University of Oregon. Specimen numbers are University of Oregon paleontology conodont specimens (UOPS). These conodonts

https://doi.org/10.1017/jpa.2018.96 Published online by Cambridge University Press

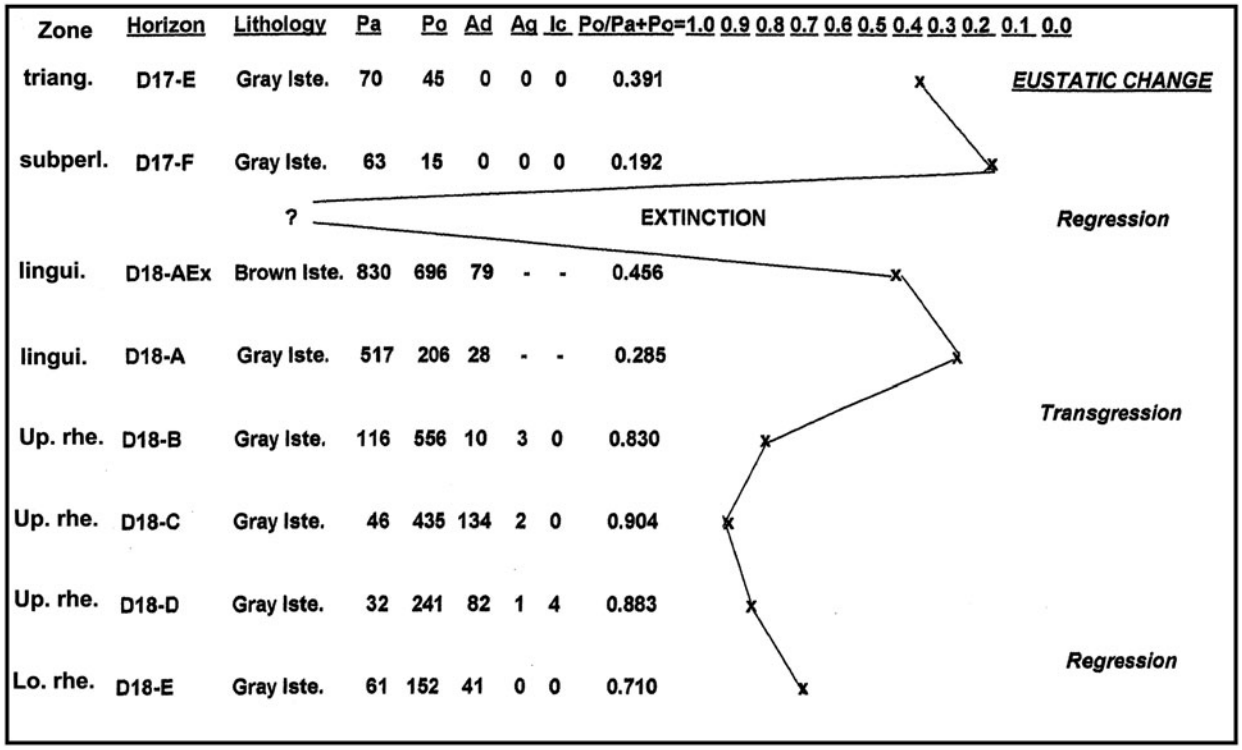


Figure 3. *Palmatolepis* (Pa.), *Polygnathus* (Po.), *Ancyrodella* (Ad.), *Ancyrognathus* (Ag.), *Icriodus* (Ic.) P1 element numbers, resulting Po/Pa + Po plot, and eustatic change interpretation for the eight horizons D18-E (Lower *rhenana* Zone) up to D17-E (*triangularis* Zone).

will be assigned Condon Collection numbers by the curator after publication.

The conodont faunas

The conodont abundances refer to P1 elements. The counts of P1 elements herein and in Savage (2013) are those remaining after some were sent to G. Racki earlier for the geochemical analyses reported by Dopieralska et al. (2012), Königshof et al. (2012), and Savage (2013).

Biofacies and eustatic changes

The tectonic influences on the depositional environment are difficult to assess from the sedimentary strata. Tectonic workers have suggested the Mae Sariang area probably belongs to the Sibumasu Terrane or to the adjacent Inthanon Zone (Kamata et al., 2009; Metcalfe, 2011). In any case, it seems likely it was in a variable deeper shelf setting in the vicinity of the eastern Paleothethys Ocean.

The succession of limestone from intervals D18 upward to D1 indicates a pelagic, mostly deepwater environment with a slow accumulation of algal carbonate particles during a 16 million year period from the late Frasnian to the late Famennian. The 18 or more bedding planes presumably indicate sedimentary breaks although most conodont zones are represented, at least in part. There are probably some hiatuses that are not visible. Some discussion of the geochemistry, including the major positive δ13C isotope excursion at the Upper Kellwasser horizon, is given in Königshof et al. (2012) and Savage (2013).

The systematic assessment of conodonts from horizons D18-E up to D17-F shows that over 85% of the P1 elements belong to species of *Palmatolepis* and *Polygnathus*. These genera are not equally represented in the intervals studied. Some, in the intervals D18-E to D18-B of the Lower to Upper *rhenana* zones, are *Polygnathus*-dominated, whereas interval D17-F of the Lower *triangularis* Zone is *Palmatolepis*-dominated. Between, in intervals D18-A and D18-AEx of the *linguiformis* Zone, *Palmatolepis* and *Polygnathus* occur more equally (Fig. 3).

The biofacies concepts proposals of Sandberg (1976), Sandberg and Ziegler (1979), Ziegler and Sandberg (1990), and subsequent workers, use *Palmatolepis*-dominated and *Polygnathus*-dominated faunas to indicate water depths and sedimentary environments. The *Polygnathus-Palmatolepis* ratios in the Lower *rhenana* Zone and Upper *rhenana* Zone Mae Sariang intervals D18-E to D18-B indicate relatively regressive conditions. There is then a deepening from interval D18-B to interval D18-A. Intervals D18-A and D18-AEx are in the *linguiformis* Zone. It is immediately above interval D18-AEx and thus above the *linguiformis* Zone that the extinction event occurs (Fig. 3). This marks the Frasnian-Famennian (F-F) boundary. Many workers (see Racki, 2005) have suggested that a global glacially forced regression was responsible for this event, although Becker et al. (2016. p. 230) favor "variable euthrophication and primary productivity pulses, not the undeniable sea-level changes." Recently, some researchers (e.g., Sanei et al., 2012; Jones et al., 2016; Thibodean and Berquist, 2017) have suggested that a toxic level of marine mercury caused by widespread volcanism is a more likely explanation for several global extinction events. Increased toxic levels of

https://doi.org/10.1017/jpa.2018.96 Published online by Cambridge University Press

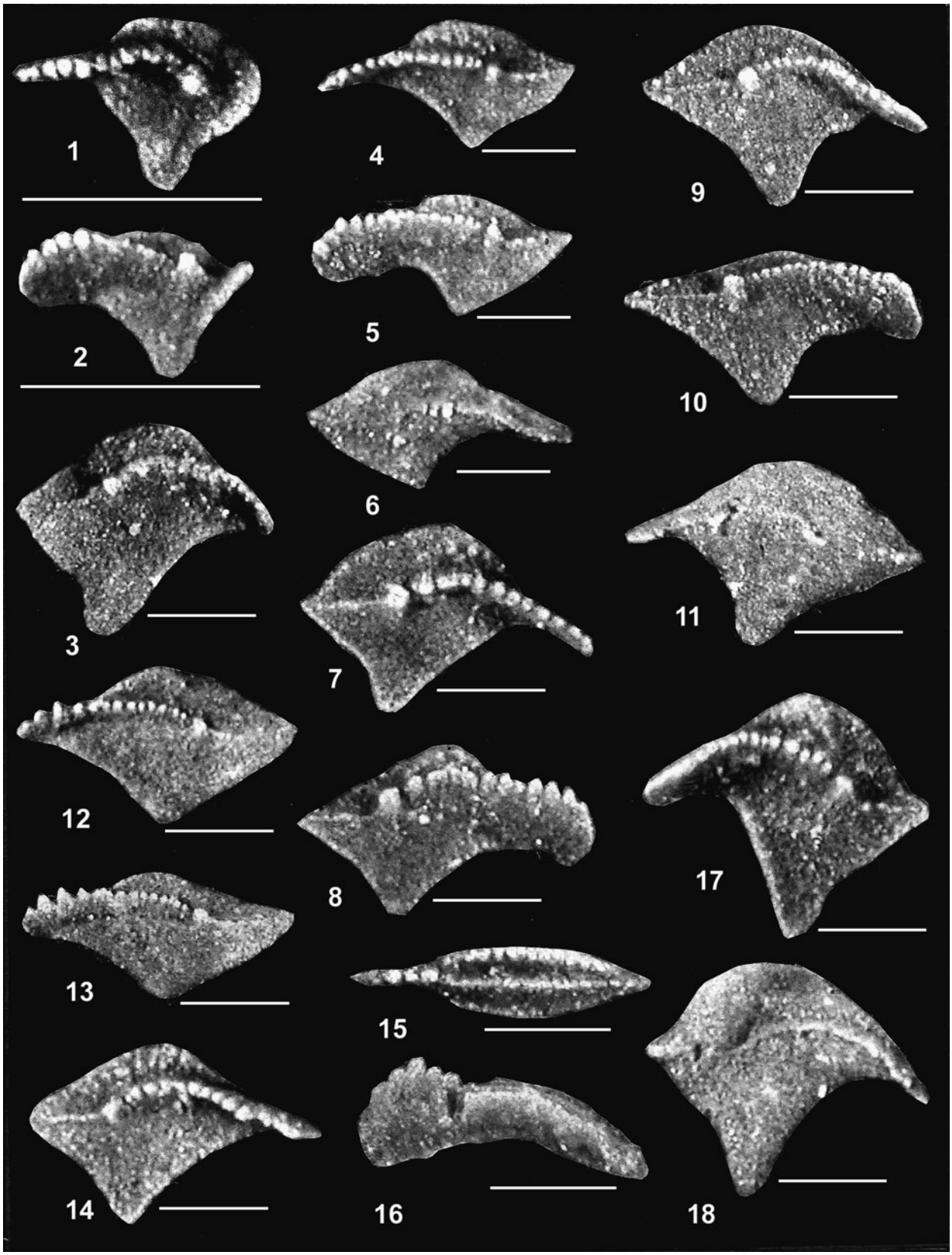
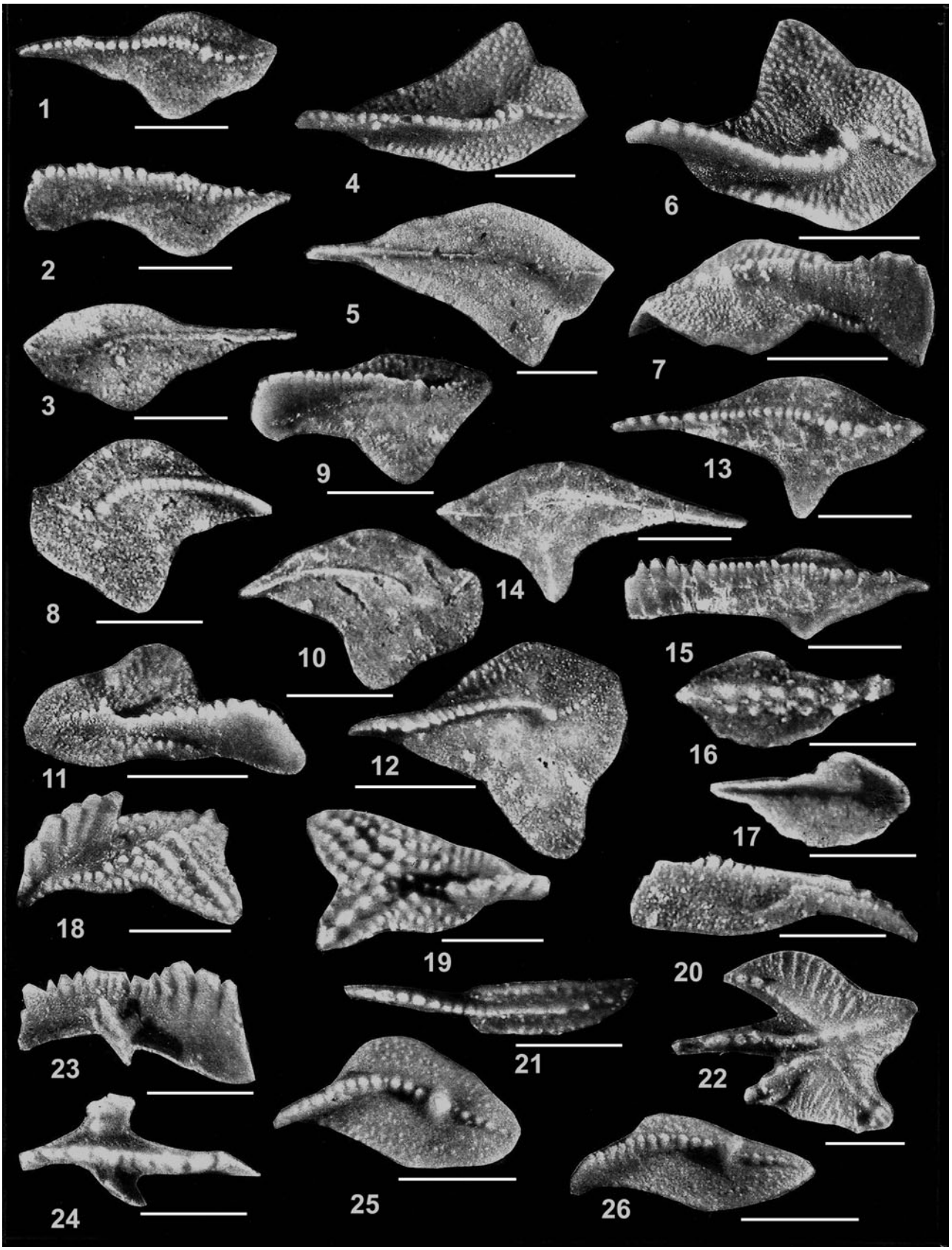


Figure 4. All specimens are from interval D17-F. (**1, 2**) *Palmatolepis* new species A, oral and oblique-lateral views of P1 element UOPS 602. (**3, 7, 8**) *Palmatolepis* aff. *Pa. triangularis* Sannemann, 1955a; (**3**) oral view of P1 element UOPS 603; (**7, 8**) oral and oblique-lateral views of P1 element UOPS 605. (4–6) *Palmatolepis triangularis* Sannemann, 1955a, oral, oblique-lateral, and aboral views of P1 element UOPS 604. (**9–11, 14**) *Palmatolepis praetriangularis* Ziegler and Sandberg, 1988; (**9–11**) oral, oblique-lateral, and aboral views of P1 element UOPS 606; (**14**) oral view of P1 element UOPS 608. (**12, 13**) *Palmatolepis werneri* Ji and Ziegler, 1993, oral and oblique-lateral views of P1 element UOPS 607. (**15, 16**) *Polygnathus procerus* Sannemann, 1955b, oral and lateral views of P1 element UOPS 609. (**17, 18**) *Palmatolepis* aff. *Pa. delicatula delicatula* Branson and Mehl, 1934, oral and aboral views of P1 element UOPS 610. Note: These conodonts, from the limestone immediately above the F-F event, are relatively few (see numbers in Fig. 3) and have a coating of detritus. Scale bars = 0.5 mm.

https://doi.org/10.1017/jpa.2018.96 Published online by Cambridge University Press



https://doi.org/10.1017/jpa.2018.96 Published online by Cambridge University Press

volcanic metals could be contributors to the F-F extinction event in the Mae Sariang area, although geochemical documentation is currently limited to that shown in figure 4a-h of Savage (2013).

The *Palmatolepis*-dominated *Palmatolepis subperlobata* Biozone and *triangularis* Zone intervals D17-F to D16-E suggest a continuing offshore, deeper-water environment. This *Palmatolepis*-dominant biofacies continues during most of the overlying Famennian beds in the Mae Sariang section from interval D17-F through to D1-A (Savage, 2013), the latter interval probably in the *Bi. ultimus* Zone of Spalletta et al. (2017).

An abrupt and distinct brownish coloration of the limestone in D18-AEx, during the second half of the *linguiformis* Zone, coincides with an increase in iron (Fe) and manganese (Mn) (see Savage, 2013, fig. 4g). The brownish limestone comprises two parts (Fig. 2.3), the lower, darker part is 9 cm thick (cf. Königshof et al., 2012), and the upper, less dark part is 7 cm thick. Both contain disarticulated shell fragments and conodonts that include *Palmatolepis linguiformis*. A photograph taken in 2010 of a field assistant standing in the same place as Figure 2.2 is fortuitous in that the brownish bed is level with the top of his cap and can be seen to be a continuous bed (Fig. 2.4). Volcanic activity, presumably local in part, was a possible cause of the sudden brownish color change, though it should be noted that *Palmatolepis linguiformis* and other conodonts continue through this interval, apparently undiminished, although showing increased morphological variation, as noted for some taxa elsewhere by Ziegler and Sandberg (1990, p. 110). The occurrence of the bottom of the brownish layers 16 cm below the extinction event is intriguing (Fig. 2.3). If the extinction event was caused by a global temperature drop and a glacially forced regression, it is difficult to explain the relevance of this sudden color change 16 cm lower, particularly as the limestone continued to accumulate and the conodont and other faunas seemingly thrived for thousands of years. Recently, several workers have suggested that major volcanic events on the Siberian Platform contributed to Late Devonian climatic changes (Racki, 2005; Kiselev et al., 2006; Courtillot et al., 2010; Bond and Grasby, 2017). These volcanics include the Viluy basalts and the Pripyat-Dniepner-Donets basalts, which were very extensive and probably injected large amounts of CO2 and other gases into the atmosphere and possibly added toxic amounts of metals to the oceans. Regardless of terrane reconstructions, it is unlikely Siberian Platform volcanics caused the brownish layers in the Mae Sariang deposits, although this does not preclude the possibility that local volcanics occurred during a time of widespread volcanism.

Detailed sedimentological discussion of the lower part of the brownish layer is included in Königshof et al. (2012), although it should be noted the thickness of the lower layer is given there as 15 cm, compared with 9 cm here. As discussed by Savage (2013, p. 7), the positive and negative excursions of δ13C in the Mae Sariang section (see Savage, 2013, fig. 3) generally match the regressions and transgressions suggested by Buggisch and Joachimski (2006).

The sequence of sampled intervals, lithology, and number of P1 elements from D17-E, above, to D18-E, below, is as follows:

D17-E gray limestone:	*triangularis* Zone, few (115) conodonts recovered in this interval
D17-F gray limestone:	*subperlobata* Zone, few (78) conodonts in this interval (Figure 4)
(Bedding plane: extinction event)	
D18-AEx brownish limestone:	upper part of *linguiformis* Zone: abundant (1,526) conodonts (Figure 5)
D18-A gray limestone:	lower part of *linguiformis* Zone: abundant (723) conodonts (Figures 6, 7)
D18-B gray limestone:	Upper *rhenana* Zone: abundant (672) conodonts (Figure 8)
D18-C gray limestone:	Upper *rhenana* Zone: numerous (481) conodonts (Figure 9)
D18-D gray limestone:	Lower *rhenana* Zone: frequent (273) conodonts (Figures 10, 11)
D18-E gray limestone:	Lower *rhenana* Zone: frequent (213) conodonts (Figure 12)

Systematic paleontology

The figure captions indicate from which intervals the described conodonts were collected.

Class Conodonti Branson, 1938
Genus *Ancyrodella* Ulrich and Bassler, 1926

Type species.—*Ancyrodella nodosa* Ulrich and Bassler, 1926 from the Rhinestreet Black Shale, Erie County, New York, by original designation.

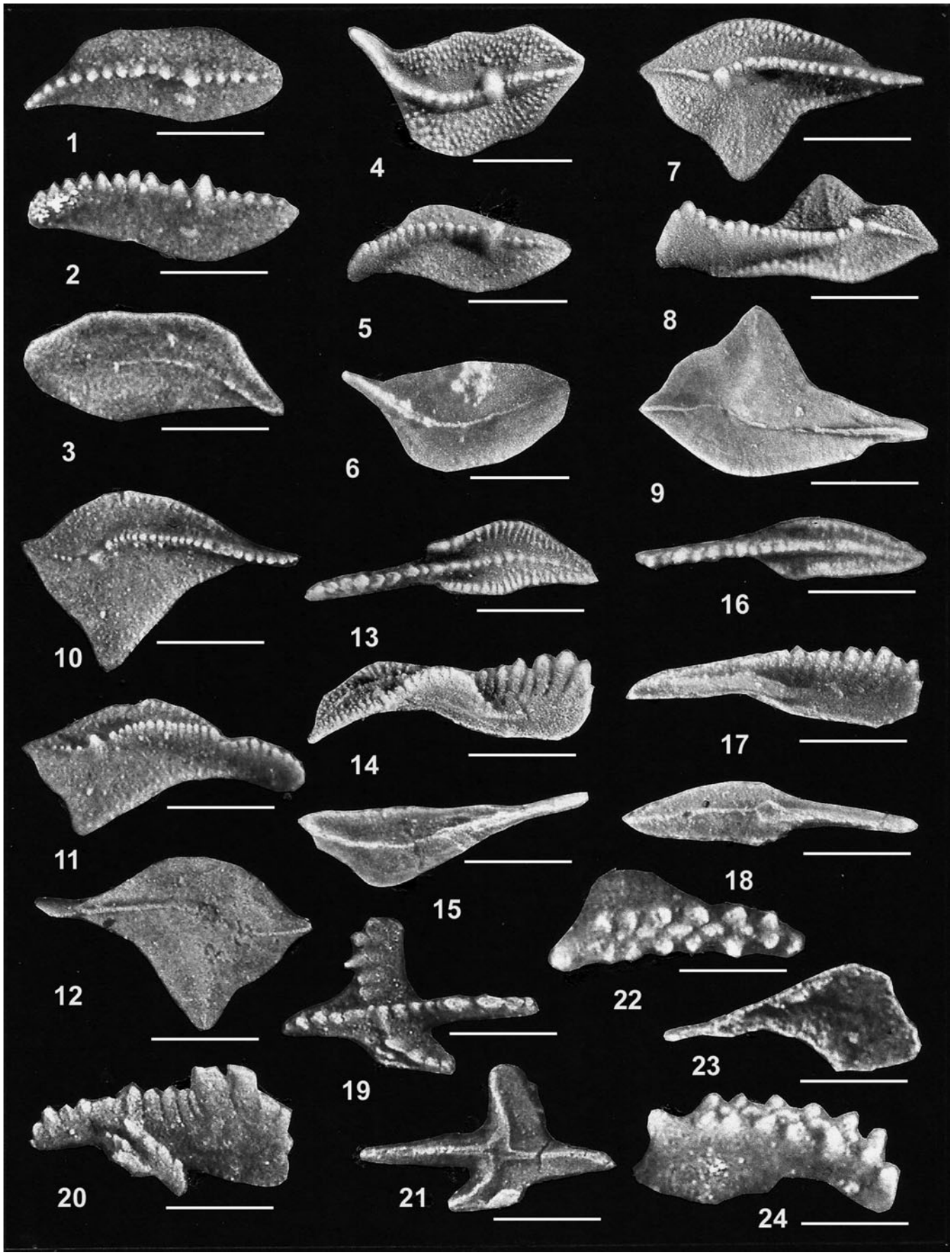
Ancyrodella curvata (Branson and Mehl, 1934)
Figures 5.22, 7.1, 7.2

Lectotype.—*Ancyrognathus curvata* Branson and Mehl, 1934 (p. 241, pl. 19, fig. 6).

Remarks.—Two morphotypes have been recognized in this species. The early morphotype (Fig. 7.1, 7.2), occurring here

Figure 5. All specimens are from interval D18-AEx. (**1–3**) *Palmatolepis chaemensis* new species, oral, lateral, and aboral views of P1 element UOPS 595, holotype. (**4, 5**) *Palmatolepis khaensis* Savage, 2013, oral and aboral views of P1 element UOPS 599. (**6, 7**) *Palmatolepis marki* Savage, 2013, oral and oblique-lateral views of P1 element UOPS 472, holotype. (**8–12**) *Palmatolepis* aff. *Pa. rotunda* Ziegler and Sandberg, 1990; (**8–10**) oral, oblique-lateral, and aboral views of P1 element UOPS 600; (**11, 12**) oblique-lateral and oral views of P1 element UOPS 596. (**13–15**) *Palmatolepis* aff. *Pa. subrecta* Miller and Youngquist, 1947, oral, aboral, and oblique-lateral views of P1 element UOPS 601. (**16, 17**) *Icriodus alternatus alternatus* Branson and Mehl, 1934, oral and aboral views of P1 element UOPS 611. (**18, 19**) *Ancyrognathus asymmetricus* (Ulrich and Bassler, 1926), oblique-lateral and oral views of P1 element UOPS 476. (**20, 21**) *Polygnathus tenellus tenellus* Ji and Ziegler, 1993, lateral and oral views of P1 element UOPS 613. (**22**) *Ancyrodella curvata* (Branson and Mehl, 1934) late morphotype, oral view of P1 element UOPS 612. (**23, 24**) *Ancyrodella ioides* Ziegler, 1958, lateral and oral views of P1 element UOPS 475. (**25, 26**) *Palmatolepis linguiformis* Müller, 1956, oral and oblique-lateral views of P1 element UOPS 479. Scale bars = 0.5 mm.

https://doi.org/10.1017/jpa.2018.96 Published online by Cambridge University Press



https://doi.org/10.1017/jpa.2018.96 Published online by Cambridge University Press

in interval D18-A, has a less developed posterolateral lobe. The late morphotype (Fig. 5.22), common here in interval D18-AEx, differs in having a posterolateral lobe bearing a secondary carina and lobe.

Ancyrodella hamata Ulrich and Bassler, 1926
Figures 7.20, 7.21, 8.22–8.24, 9.27–9.32, 11.18–11.21, 12.21–12.23

Holotype.—*Ancyrodella hamata* Ulrich and Bassler, 1926 (p. 48, pl. 7, fig. 7).

Remarks.—Abundant in intervals D18-AEx to D18-E. The species has been identified earlier by the author as *And. buckeyensis*. It is now generally accepted that *And. hamata* is a senior synonym.

Ancyrodella ioides Ziegler, 1958
Figures 5.23, 5.24, 6.19–6.21, 12.18–12.20

Holotype.—*Ancyrodella ioides* Ziegler, 1958 (p. 42, pl. 11, fig. 2a, b).

Remarks.—Forty-six specimens occur in intervals D18-AEx, D18-A, and D18-E. Compared with other species of *Ancyrodella*, the platform is much reduced, the lateral blades curved anteriorly, and the denticles of the blade anterior are high.

Genus *Ancyrognathus* Branson and Mehl, 1934

Type species.—*Ancyrognathus symmetricus* Branson and Mehl, 1934 from the Sees Creek locality, Saveton Shale, Marion County, Missouri, by original designation.

Ancyrognathus asymmetricus (Ulrich and Bassler, 1926)
Figure 5.18, 5.19

Holotype.—*Palmatolepis asymmetrica* Ulrich and Bassler, 1926 (p. 50, pl. 7, fig. 18).

Remarks.—In this species the lateral lobe is directed posterolaterally; the blade is short and particularly high anteriorly.

Ancyrognathus aff. *Ag. barbus* Sandberg and Ziegler 1992
Figure 11.10, 11.11

Holotype.—*Ancyrognathus barbus* Sandberg and Ziegler, 1992 (p. 52, pl. 7, figs. 4, 5).

Remarks.—The figured specimen differs from the holotype and other figured specimens of Sandberg and Ziegler, 1992 in having a lateral carina without the marked anterior curvature and in having a much narrower platform. The holotype of *Ag. barbus* is from the upper *Palmatolepis hassi* Zone.

Genus *Icriodus* Branson and Mehl, 1938

Type species.—*Icriodus expansus* Branson and Mehl, 1938 from the Mineola Limestone, Montgomery County, Missouri, by original designation.

Icriodus alternatus alternatus Branson and Mehl, 1934
Figures 5.16, 5.17, 6.22–6.24, 11.1–11.3

Lectotype.—*Icriodus alternatus* Branson and Mehl, 1934 (p. 225, pl. 13, fig. 4), selected by Ziegler (1962, p. 51).

Remarks.—The lectotype selected by Ziegler (1962) has a broken posterior cusp. Szulczewski's (1971) discussion of the taxon noted the divergence of various authors' interpretations. Klapper (1975) suggested that weak middle row denticles may be more characteristic than the alternation of lateral denticles in the taxon.

Genus *Palmatolepis* Ulrich and Bassler, 1926

Type species.—*Palmatolepis perlobata* Ulrich and Bassler, 1926 from the Hardin Sandstone, Maury County, Tennessee, by original designation.

Palmatolepis amplificata Klapper, Kuz'min, and Ovnatanova, 1996
Figure 7.3–7.5, 7.9, 7.10

Holotype.—*Palmatolepis amplificata* Klapper, Kuz'min, and Ovnatanova, 1996 (p. 140, fig. 7.2).

Remarks.—The specimens have a broader outer lobe than the holotype, but the high anterior blade, inner lobe parapet, weak lateral carina, and strong uniform denticles indicate this species.

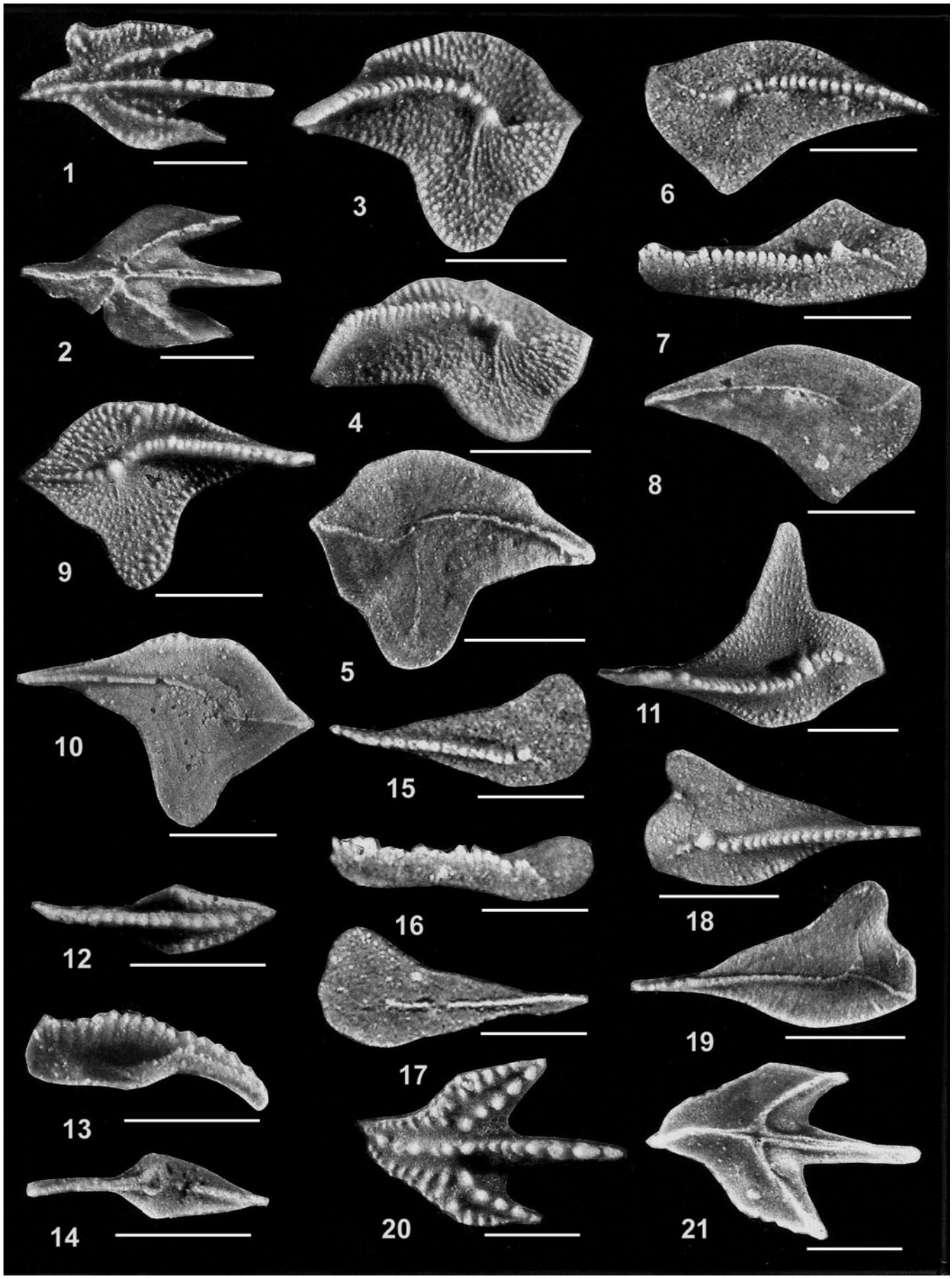
Palmatolepis aff. *Pa. boogaardi* Klapper and Foster, 1993
Figure 10.10–10.12

Remarks.—This specimen has a weaker lobe than the holotype of Klapper and Foster (1993) and alternatively could be assigned to *Pa. hassi* Müller and Müller (1957), broadly interpreted.

Palmatolepis chaemensis new species
Figure 5.1–5.3

Figure 6. All specimens are from interval D18-A. (**1–6**) *Palmatolepis linguiformis* Müller, 1956; (**1–3**) oral, lateral, and aboral views of P1 element UOPS 584; (4–6) oral, oblique-lateral, and aboral views of P1 element UOPS 487. (**7–9**) *Palmatolepis hassi* Müller and Müller, 1957, oral, oblique-lateral, and aboral views of P1 element UOPS 480. (**10–12**) *Palmatolepis* aff. *Pa. kireevae* Ovnatanova, 1976, oral, oblique-lateral, and aboral views of P1 element UOPS 586. (**13–15**) *Polygnathus burretti* Savage, 2013, oral, lateral, and aboral views of P1 element UOPS 490, holotype. (**16–18**) *Polygnathus tenellus tenellus* Ji and Ziegler, 1993, oral, lateral, and aboral views of P1 element UOPS 587. (**19–21**) *Ancyrodella ioides* Ziegler, 1958, oral, lateral, and aboral views of P1 element UOPS 588. (**22–24**) *Icriodus alternatus alternatus* Branson and Mehl, 1934, oral, aboral, and lateral views of P1 element UOPS 589. Scale bars = 0.5 mm.

https://doi.org/10.1017/jpa.2018.96 Published online by Cambridge University Press



https://doi.org/10.1017/jpa.2018.96 Published online by Cambridge University Press

Holotype.—P1 element UOPS 595, the specimen illustrated in Figure 5.1–5.3. Repository: Condon Collection, University of Oregon.

Diagnosis.—Palmatolepid having a P1 element with a straight blade bearing small confluent denticles and a long narrow platform that is up-flexed posteriorly.

Description.—A straight to slightly sinuous blade is composed of small confluent denticles. A long narrow platform has its greatest width at about unit midlength, with a sinuous outer margin commencing near the anterior of the blade, a short outer lobe at about midlength, situated anterior of the main node, and a slight sinus just posterior of the main node. The main node is not prominent. The inner platform margin commences just anterior of unit midlength. The platform surface is smooth, and the posterior of the platform is up-flexed. Aborally a very small basal pit is located below the main node.

Etymology.—After Mae Chaem, a village northeast of the town of Mae Sariang.

Materials.—Holotype plus five paratypes.

Remarks.—The new species bears some resemblance to *Palmatolepis minuta* Branson and Mehl (1934) from several zones higher, but is not close to known late *linguiformis* Zone taxa.

Palmatolepis aff. *Pa. delicatula delicatula* Branson and Mehl, 1934
Figure 4.17, 4.18

Remarks.—In this taxon, the outer lobe is large and directed slightly anterior of the node.

Palmatolepis hassi Müller and Müller, 1957
Figure 6.7–6.9

Holotype.—*Palmatolepis (Manticolepis) hassi* Müller and Müller, 1957 (p. 1103, pl. 140, fig. 4a–c).

Remarks.—*Pa. hassi* occurs in the Mae Sariang section from the Lower *rhenana* Zone into the *linguiformis* Zone, where it is abundant (see Savage, 2013, table 3).

Palmatolepis aff. *Pa. hassi* Müller and Müller, 1957
Figure 9.24–9.26

Remarks.—The figured specimens are smoother than the P1 element of *Pa. hassi* Müller and Müller (1957), have a smaller lateral lobe, and lack the inner and outer sinuses near the posterior tip of the platform. They differ from the P1 element of *Pa. zhuravlevi* Soboleva (2017) in having a less rounded posterior platform.

Palmatolepis jamieae Ziegler and Sandberg, 1990
Figure 12.13–12.15

Holotype.—*Palmatolepis jamieae* Ziegler and Sandberg, 1990 (p. 50, pl. 6, fig. 1–3).

Remarks.—This species is characterized by a flattish to slightly arched platform with maximum width just anterior of the main node, a broad outer lobe, and a straight blade that is high anteriorly and merges posteriorly into a sinuous carina. The taxon ranges from the *Palmatolepis jamieae* Zone to the Lower *rhenana* Zone.

Palmatolepis aff. *Pa. jamieae* Ziegler and Sandberg, 1990
Figure 9.3–9.5

Remarks.—This specimen is elongate for *Pa. jamieae*. D18-C is a little high for the taxon range.

Palmatolepis juntianensis Han, 1987
Figure 7.15–7.17

Holotype.—*Palmatolepis juntianensis* Han, 1987 (p. 186, pl. 1, fig. 15).

Remarks.—The figured specimen is very like the holotype of Han (1987).

Palmatolepis khaensis Savage, 2013
Figures 5.4, 5.5, 7.18, 7.19, 12.16, 12.17

Holotype.—*Palmatolepis khaensis* Savage, 2013 (p. 17, fig. 7.4–7.6).

Remarks.—The specimen in Figure 5.4, 5.5 is a reillustrated paratype from Savage (2013).

Palmatolepis cf. *Pa. kireevae* Ovnatanova, 1976
Figure 10.7–10.9

Holotype.—*Palmatolepis kireevae* Ovnatanova, 1976 (p. 215, pl. 9, fig. 5a, b).

Remarks.—The lobe tip of this specimen is directed less anteriorly than that in the holotype.

Palmatolepis aff. *Pa. kireevae* Ovnatanova, 1976
Figure 6.10–6.12

Figure 7. All specimens are from interval D18-A. (**1, 2**) *Ancyrodella curvata* (Branson and Mehl, 1934) early morphotype, oral and aboral views of P1 element UOPS 590. (**3–5, 9, 10**) *Palmatolepis amplificata* Klapper, Kuz'min, and Ovnatanova, 1996; (**3–5**) oral, oblique-lateral, and aboral views of P1 element UOPS 591; (**9, 10**) oral and aboral views of P1 element UOPS 593. (**6–8**) *Palmatolepis* cf. *Pa. rotunda* Ziegler and Sandberg, 1990, oral, oblique-lateral, and aboral views of P1 element UOPS 592. (**11**) *Palmatolepis nasuta* Müller, 1956, oral view of P1 element UOPS 484. (**12–14**) *Polygnathus tenellus tenellus* Ji and Ziegler, 1993, oral, lateral, and aboral views of P1 element UOPS 489. (**15–17**) *Palmatolepis juntianensis* Han, 1987, oral, lateral, and aboral views of P1 element UOPS 594. (**18, 19**) *Palmatolepis khaensis* Savage, 2013, oral and aboral views of P1 element UOPS 483. (**20, 21**) *Ancyrodella hamata* Ulrich and Bassler, 1926, oral and aboral views of P1 element UOPS 492. Scale bars = 0.5 mm.

https://doi.org/10.1017/jpa.2018.96 Published online by Cambridge University Press

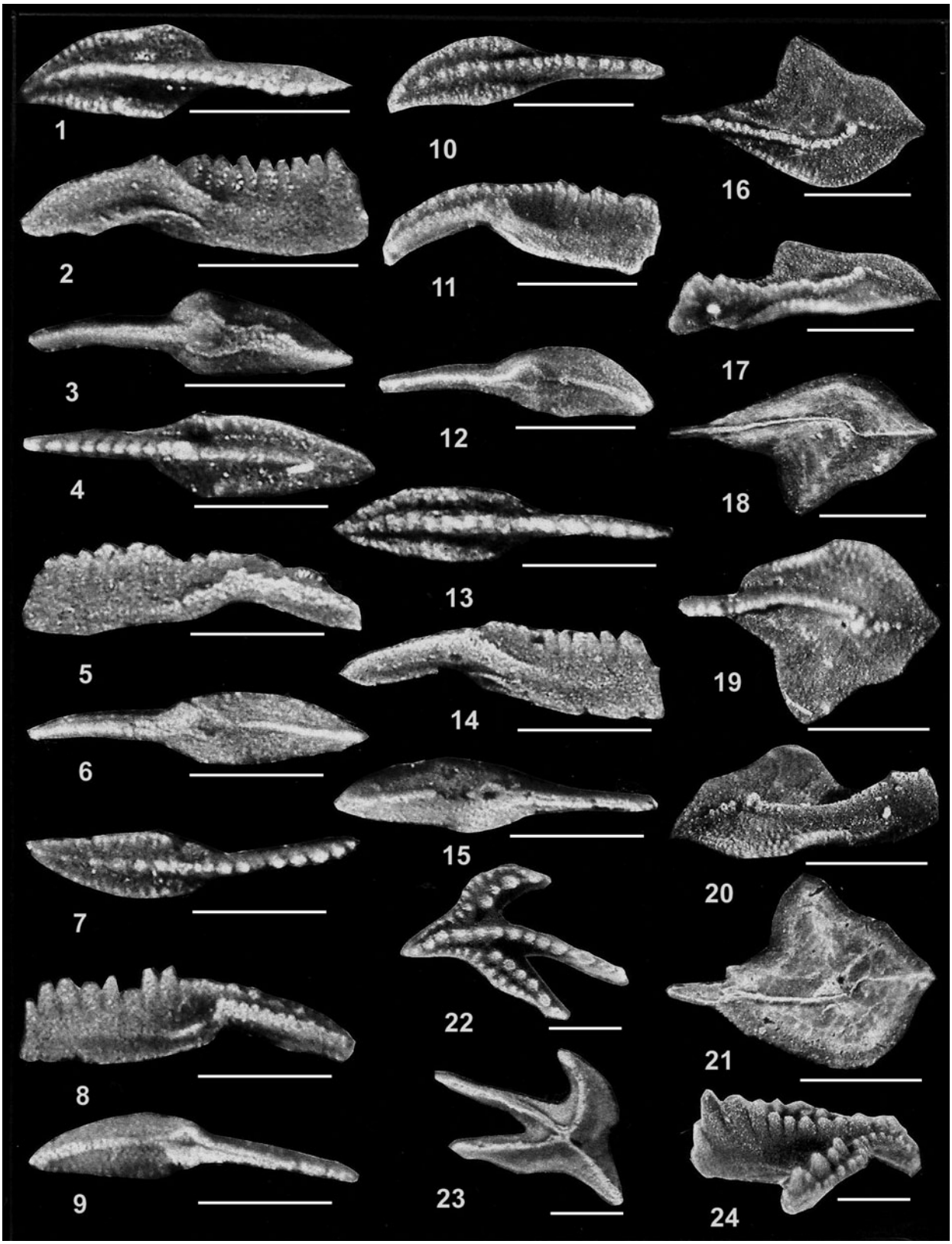
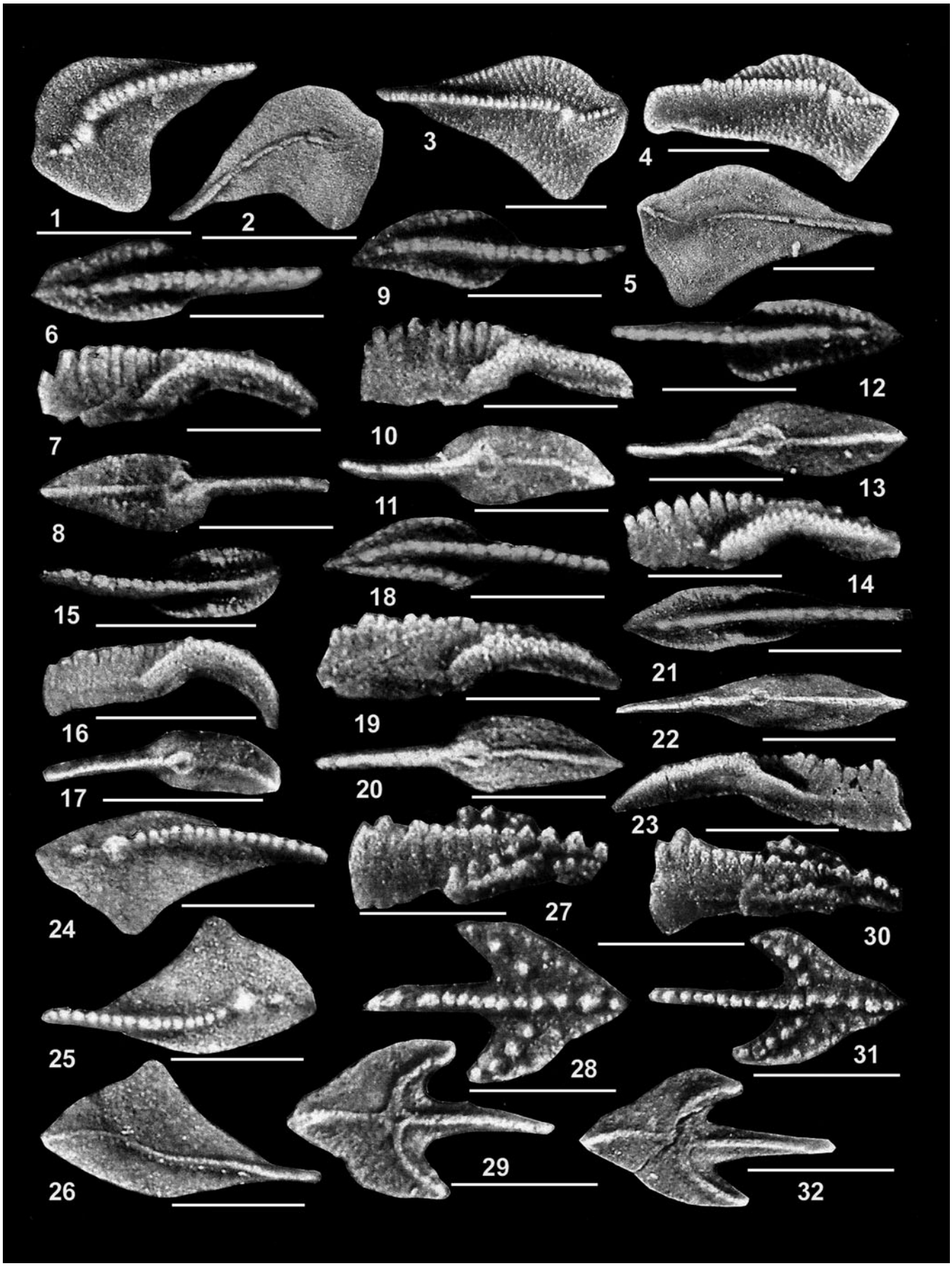


Figure 8. All specimens are from interval D18-B. (**1–3**) *Polygnathus tenellus surinensis* new subspecies, oral, lateral, and aboral views of P1 element UOPS 577. (**4–15**) *Polygnathus tenellus tenellus* Ji and Ziegler 1993; (**4–6**) oral, lateral, and aboral views of P1 element UOPS 578; (**7–9**) oral, lateral, and aboral views of P1 element UOPS 579; (**10–12**) oral, lateral, and aboral views of P1 element UOPS 580; (**13–15**) oral, lateral, and aboral views of P1 element UOPS 581. (**16–21**) *Palmatolepis marki* Savage, 2013; (**16–18**) oral, lateral, and aboral views of P1 element UOPS 582; (**19–21**) oral, oblique-lateral, and aboral views of P1 element UOPS 583. (**22–24**) *Ancyrodella hamata* Ulrich and Bassler, 1926, oral, aboral, and lateral views of P1 element UOPS 494. Scale bars = 0.5 mm.

https://doi.org/10.1017/jpa.2018.96 Published online by Cambridge University Press



https://doi.org/10.1017/jpa.2018.96 Published online by Cambridge University Press

Remarks.—The figured specimen resembles *Pa. kireevae* Ovnatanova (1976). Klapper et al. (1996, p. 145–147) described the lobe as directed slightly to the anterior. This is not so in the four specimens in D18-A. These also could be compared with *Pa.* aff. *Pa. hassi* Müller and Müller (1957) or *Pa.* aff. *Pa. wildungensis* Müller (1956).

Palmatolepis linguiformis Müller, 1956
Figures 5.25, 5.26, 6.1–6.6

Holotype.—Palmolepis linguiformis Müller, 1956 (p. 24, pl. 7, fig. 4).

Remarks.—The illustrated specimen from D18-A (Fig. 6.1–6.3) has a long platform. In the collection specimens there appears to be a gradation from those with a long platform to those with the more usual short platform, as in Figures 5.25, 5.26, 6.4–6.6.

Palmatolepis marki Savage, 2013
Figures 5.6, 5.7, 8.16–8.21

Holotype.—Palmatolepis marki Savage, 2013 (p. 19, fig. 7.7–7.9).

Remarks.—The specimen in Figure 6.10–6.12 is the reillustrated holotype from Savage (2013).

Palmatolepis nasuta Müller, 1956
Figure 7.11

Holotype.—Palmatolepis (Manticolepis) nasuta Müller, 1956 (p. 23, pl. 6, fig. 31a–c).

Remarks.—This specimen is one of several from interval D18-A with an extended lateral lobe. An even more extended lateral lobe is present in *Pa. salibaevi* Bardashev, 2009.

Palmatolepis praetriangularis Ziegler and Sandberg, 1988
Figure 4.9–4.11, 4.14

Holotype.—Palmatolepis praetriangularis Ziegler and Sandberg, 1988 (p. 298, pl. 1, fig. 1a, b).

Remarks.—The illustrated specimens are very close to the holotype of *Pa. praetriangularis* Ziegler and Sandberg (1988), a species considered a synonym of *Pa. ultima* by Klapper (2007).

Palmatolepis aff. *Pa. rotunda* Ziegler and Sandberg, 1990
Figures 5.8–5.12, 9.1, 9.2, 12.24–12.26

Holotype.—Palmatolepis rotunda Ziegler and Sandberg, 1990 (p. 62, pl. 10, fig. 3).

Remarks.—The specimen in Figure 5.7–5.9 has a larger lobe than the holotype of Ziegler and Sandberg (1990, pl. 10, fig. 3). The specimen in Figure12.24–12.26, reillustrated from Savage (2013), is possibly gerontic and has an even larger lobe and an anterior inner parapet.

Palmatolepis cf. *Pa. rotunda* Ziegler and Sandberg, 1990
Figure 7.6–7.8

Remarks.—This figured specimen could be an immature *Pa. rotunda* Ziegler and Sandberg (1990) but with a weak outer lobe.

Palmatolepis aff. *Pa. subrecta* Miller and Youngquist, 1947
Figure 5.13–5.15

Remarks.—This specimen is longer and has the lobe more anteriorly placed than in the lectotype, selected by Müller and Müller (1957, p. 1104).

Palmatolepis thamensis new species
Figure 10.1–10.6

Holotype.—P1 element UOPS 554; the specimen illustrated in Figure 10.1–10.3. Repository: Condon Collection, University of Oregon.

Diagnosis.—A palmatolepid having a P1 element with the outer lobe tip narrowly rounded and posteriorly deflected.

Description.—The P1 element is subtriangular, with the inner platform margin evenly convex and the outer margin sinuous. The posterior outer margin is arched. The outer lobe tip is deflected posteriorly. The platform surface is smooth to finely nodose. The blade extends only slightly anterior of the platform. The blade and anterior carina are distinctly curved and bear strong, even denticles, extending to a prominent main node. The posterior carina reaches the posterior of the unit and comprises a variable number of fine nodes. Aborally, a minute basal pit occurs beneath the main node.

Etymology.—After Na Tham village, east of the town of Mae Sariang.

Materials.—Holotype and three paratypes.

Remarks.—The new species has some resemblance to *Pa. kireevae* Ovnatanova (1976) but differs in the rounded and posteriorly deflected outer lobe. *Pa. hassi* Müller and Müller (1957) has a wider, more evenly rounded outer lobe and coarse nodes on the anterior of the inner lobe.

Figure 9. All specimens are from interval D18-C. (**1, 2**) *Palmatolepis* aff. *Pa. rotunda* Ziegler and Sandberg, 1990, oral and aboral views of P1 element UOPS 497. (**3–5**) *Palmatolepis* aff. *Pa. jamieae* Ziegler & Sandberg, 1990, oral, oblique-lateral, and aboral views of P1 element UOPS 499. (**6–11, 18–20**) *Polygnathus tenellus tenellus* Ji and Ziegler, 1993; (**6–8**) oral, lateral, and aboral views of P1 element UOPS 568; (**9–11**) oral, lateral, and aboral views of P1 element UOPS 569, holotype; (**18–20**) oral, lateral, and aboral views of P1 element UOPS 572. (**12–14**) *Polygnathus tenellus surinensis* new subspecies, oral, lateral, and aboral views of P1 element UOPS 570. (**15–17**) *Polygnathus* aff. *Po. procerus* Sannemann, 1955b, oral, lateral, and aboral views of UOPS P1 element 571. (**21–23**) *Polygnathus politus* Ovnatanova, 1969, oral, lateral, and aboral views of P1 element UOPS 573. (**24–26**) *Palmatolepis* aff. *Pa. hassi* Müller and Müller, 1957, oblique-lateral, oral, and aboral views of P1 element UOPS 574. (**27–32**) *Ancyrodella hamata* Ulrich and Bassler, 1926; (**27–29**) lateral, oral, and aboral views of P1 element UOPS 575; (**30–32**) lateral, oral, and aboral views of P1 element UOPS 576. Scale bars = 0.5 mm.

https://doi.org/10.1017/jpa.2018.96 Published online by Cambridge University Press

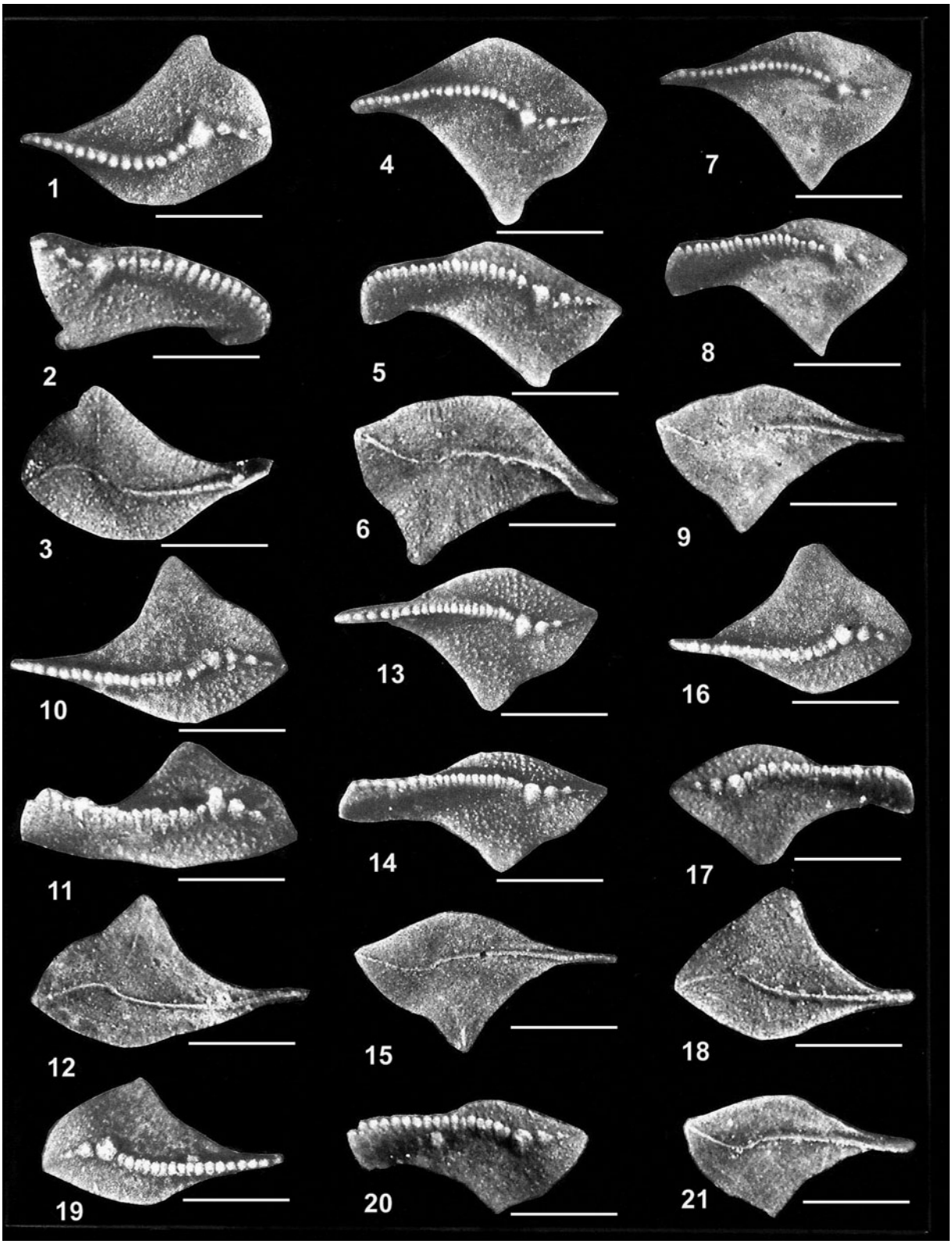


Figure 10. All specimens are from interval D18-D. (**1–6**) *Palmatolepis thamensis* new species; (**1–3**) oral, lateral, and aboral views of P1 element UOPS 554, holotype; (**4–6**) oral, lateral, and aboral views of P1 element UOPS 555, paratype. (**7–9**) *Palmatolepis* cf. *Pa. kireevae* Ovnatanova, 1976, oral, lateral-oblique, and aboral views of P1 element UOPS 556. (**10–12**) *Palmatolepis* aff. *Pa. boogaardi* Klapper and Foster, 1993, oral, lateral-oblique, and aboral views of P1 element UOPS 557. (**13–18**) *Palmatolepis* new species B; (**13–15**) oral, lateral-oblique, and aboral views of P1 element UOPS 558; (**16–18**) oral, lateral-oblique, and aboral views of P1 element UOPS 559. (**19–21**) *Palmatolepis thanisi* Savage, Sardsud, and Buggisch, 2006, oral, lateral-oblique, and aboral views of P1 element UOPS 560. Scale bars = 0.5 mm.

https://doi.org/10.1017/jpa.2018.96 Published online by Cambridge University Press

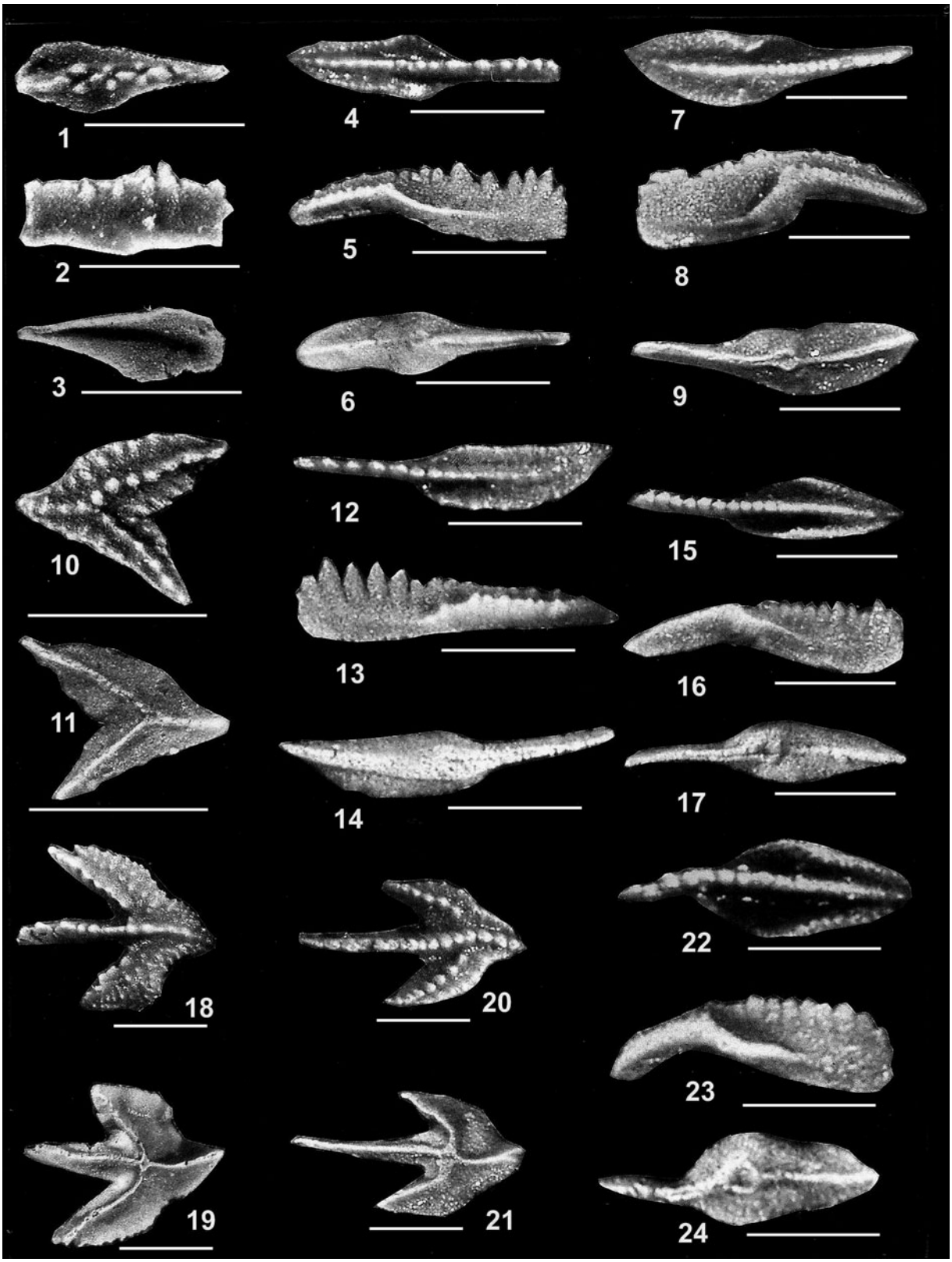


Figure 11. All specimens are from interval D18-D. (**1–3**) *Icriodus alternatus alternatus* Branson and Mehl, 1934, oral, lateral, and aboral views of P1 element UOPS 500. (**4–6, 12–14**) *Polygnathus tenellus tenellus* Ji and Ziegler, 1993; (**4–6**) oral, lateral, and aboral views of P1 element UOPS 561; (**12–14**) oral, lateral, and aboral views of P1 element UOPS 563. (**7–9, 15–17**) *Polygnathus politus* Ovnatanova, 1969; (**7–9**) oral, lateral, and aboral views of P1 element UOPS 562; (**15–17**) oral, lateral, and aboral views of P1 element UOPS 564. (**10, 11**) *Ancyrognathus* aff. *Ag. barbus* Sandberg and Ziegler, 1992, oral and aboral views of P1 element UOPS 501. (**18–21**) *Ancyrodella hamata* Ulrich and Bassler, 1926; (**18, 19**) oral and aboral views of P1 element UOPS 565; (**20, 21**) oral and aboral views of P1 element UOPS 566. (**22–24**) *Polygnathus lodinensis* Pölsler, 1969, oral, lateral, and aboral views of P1 element UOPS 567. Scale bars = 0.5 mm.

https://doi.org/10.1017/jpa.2018.96 Published online by Cambridge University Press

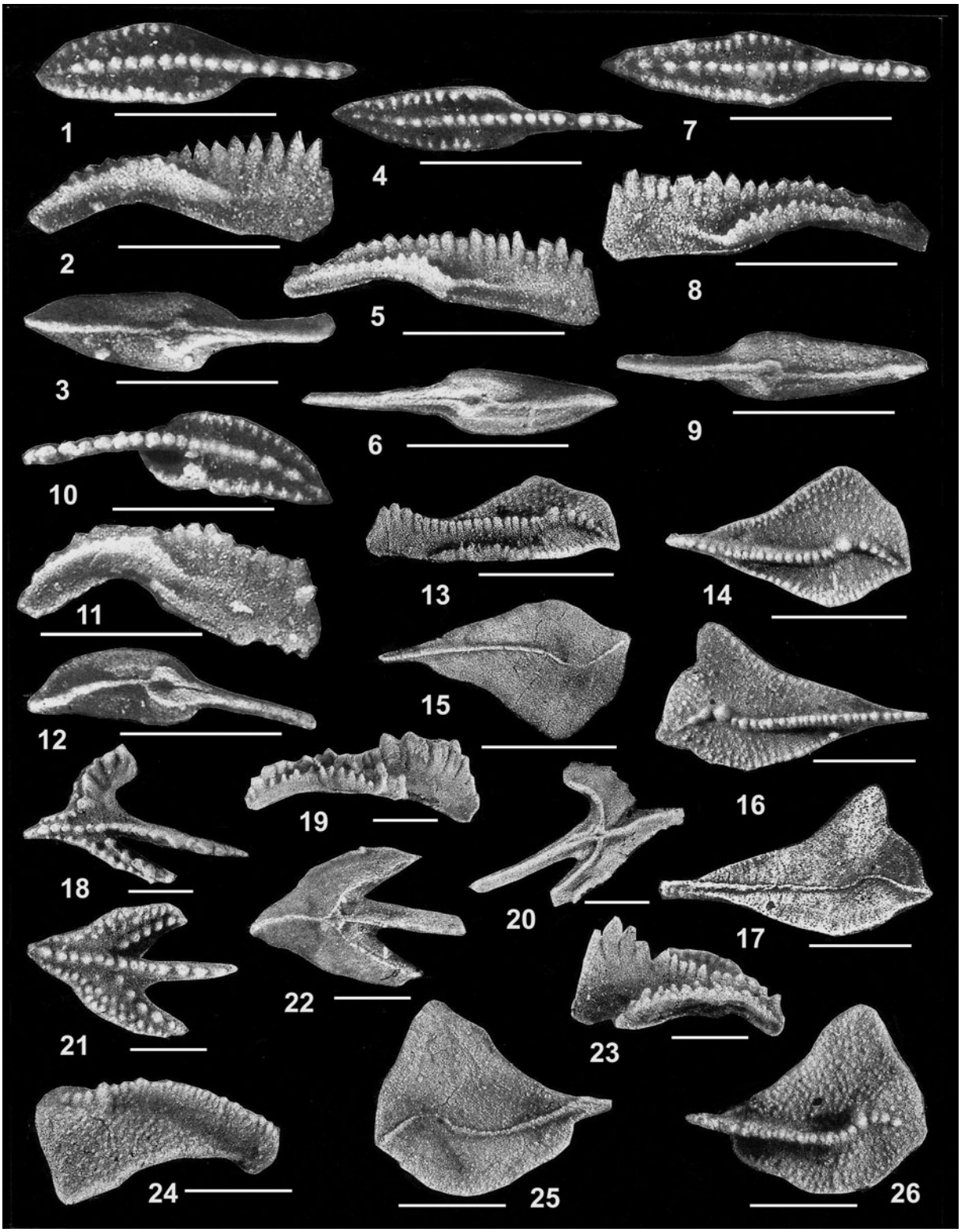


Figure 12. All specimens are from interval D18-E. (**1–12**) *Polygnathus tenellus tenellus* Ji and Ziegler, 1993; (**1–3**) oral, lateral, and aboral views of P1 element UOPS 550; (**4–6**) oral, lateral, and aboral views of P1 element UOPS 551; (**7–9**) oral, lateral, and aboral views of P1 element UOPS 552; (**10–12**) oral, lateral-oblique, and aboral views of P1 element UOPS 553. (**13–15**) *Palmatolepis jamieae* Ziegler and Sandberg, 1990, lateral-oblique, oral, and aboral views of P1 element UOPS 502. (**16, 17**) *Palmatolepis khaensis* Savage, 2013, oral and aboral views of P1 element UOPS 505. (**18–20**) *Ancyrodella ioides* Ziegler, 1958, oral, lateral, and aboral views of P1 element UOPS 503. (**21–23**) *Ancyrodella hamata* Ulrich and Bassler, 1926, oral, aboral, and lateral views of P1 element UOPS 504. (**24–26**) *Palmatolepis* aff. *Pa. rotunda* Ziegler and Sandberg, 1990, lateral, aboral, and oral views of P1 element UOPS 506. Scale bars = 0.5 mm.

https://doi.org/10.1017/jpa.2018.96 Published online by Cambridge University Press

Palmatolepis thanisi Savage, Sardsud, and Buggisch, 2006
Figure 10.19–10.21

Holotype.—Palmatolepis thanisi Savage, Sardsud, and Buggisch, 2006 (p. 182, fig. 6D–F).

Remarks.—The holotype from Thong Pha Phum, Thailand (Savage et al., 2006, fig. 6D–F), was photographed (by the author) with low-angle lighting that enhanced the small nodes of the platform margin and outer lobe tip. Paratypes from Thong Pha Phum and the Mae Sariang specimens from interval D18-D herein have a relatively smooth platform surface.

Palmatolepis triangularis Sannemann, 1955a
Figure 4.4–4.6

Holotype.—Palmatolepis triangularis Sannemann, 1955a (p. 327, pl. 24, fig. 3).

Remarks.—The taxon is within a broad definition of *Pa. triangularis* Sannemann, 1955a but has a shorter platform of which the inner lobe meets the blade more posteriorly than in the holotype. It may be transitional from *Pa. praetriangularis* Ziegler and Sandberg (1988).

Palmatolepis aff. *Pa. triangularis* Sannemann, 1955a
Figure 4.3, 4.7, 4.8

Remarks.—The illustrated specimens differ from *Pa. ultima* Ziegler (1958) in having a lobe that is more rounded than in the holotype of that species and is more posteriorly directed. They differ from Ji and Ziegler's (1993) morphotype 1 of *Pa. subperlobata* Branson and Mehl (1934) in having strong nodes on the inner platform.

Palmatolepis werneri Ji and Ziegler, 1993
Figure 4.12, 4.13

Holotype.—Palmatolepis werneri Ji and Ziegler, 1993 (p. 73, pl. 22, fig. 8).

Remarks.—This species was recorded by Savage (2013) from intervals D17-F to D10-A at Mae Sariang (Savage 2013, figs. 8.19–8.21, 9.14–9.16, 11.10–11.12, tables 2, 3). The figured specimen herein closely resembles the holotype (Ji and Ziegler, 1993, pl. 22, figs. 8–11).

Palmatolepis new species A
Figure 4.1, 4.2

Remarks.—The illustrated specimen differs from known Lower *triangularis* Zone species of *Palmatolepis*. It is probably a new taxon but there are only two specimens, insufficient material to assess this. The figured specimen is small but probably not a juvenile because the other is almost twice as large. The latter was not photographed because of surface debris.

Palmatolepis new species B
Figure 10.13–10.18

Remarks.—This is a palmatolepid having a P1 element with a subtriangular outline, a mostly smooth platform with fine nodes on a raised inner margin, a rounded to subangular outer lobe, a blade with numerous confluent denticles, a conspicuous main node, and a posterior carina of few discrete denticles. The species is without the posterior inner and outer sinuses of *Pa. hassi* Müller and Müller (1957) and the high anterior blade and pointed lobe of *Pa. wildungensis* Müller (1956). It is also without the extended and broader lateral lobe of *Pa. prominens* Müller (1956) and lacks the marked post-lobe sinuses of the holotypes of *Pa. orlovi* Khrustcheva and Kuz'min (1996), *Pa. ultima* Ziegler (1958), *Pa. boogaardi* Klapper and Foster (1993), *Pa. superlobata* Branson and Mehl (1934), and *Pa. nasuta* Müller (1956). The new species might be compared with *Pa. praetriangularis* Ziegler and Sandberg (1988), from which it differs mostly in lacking the fused posterior carina denticles and having a much weaker post-lobe sinus. The material comprises 12 P1 elements from the D18-D interval and one from the D18-C interval.

Genus *Polygnathus* Hinde, 1879

Type species.—Polygnathus dubius Hinde, 1879 from the North Evans Limestone, Erie County, New York, by subsequent designation of Miller, 1889.

Polygnathus burretti Savage, 2013
Figure 6.13–6.15

Holotype.—Polygnathus burretti Savage, 2013 (p. 27, fig. 6.20–6.22).

Remarks.—The specimen is the reillustrated holotype of Savage (2013).

Polygnathus lodinensis Pölsler, 1969
Figure 11.22–11.24

Holotype.—Polygnathus lodinensis Pölsler, 1969 (p. 425, pl. 6, figs. 1–3).

Remarks.—The figured specimen and five others in the D18-D collection are very like the holotype of Pölsler (1969).

Polygnathus politus Ovnatanova, 1969
Figures 9.21–9.23, 11.7–11.9, 11.15–11.17

Holotype.—Polygnathus politus Ovnatanova, 1969 (p. 140, pl. 1, fig. 4).

Remarks.—Po. politus of Ovnatanova (1969) is the senior synonym of *Po. pacificus* Savage and Funai (1980).

Polygnathus procerus Sannemann, 1955b
Figure 4.15, 4.16

Holotype.—Polygnathus procerus Sannemann, 1955b (p. 150, pl. 1, fig. 11a, b).

https://doi.org/10.1017/jpa.2018.96 Published online by Cambridge University Press

Remarks.—In oral and lateral views, the specimen in Figure 4.15, 4.16 is close to the holotype of Sannemann (1955b). *Po. procerus* differs from *Po. tenellus* Ji and Ziegler (1993) in its more down-curved and wider platform, lower carina, and lack of a short posterior blade.

Polygnathus aff. *Po. procerus* Sannemann 1955b
Figure 9.15–9.17

Remarks.—The figured specimen has a platform that is more down-curved than that in the holotype.

Polygnathus tenellus tenellus Ji and Ziegler, 1993
Figures 5.20, 5.21, 6.16–6.18, 7.12–7.14, 8.4–8.15, 9.6–9.11, 9.18–9.20, 11.4–11.6, 11.12–11.14, 12.1–12.12

Holotype.—*Polygnathus tenellus* Ji and Ziegler, 1993 (p. 85, pl. 37, figs. 12, 13).

Remarks.—The holotype of Ji and Ziegler (1993) has a down-curved lanceolate platform (also in their paratype, pl. 37, fig. 9). This agrees with their diagnosis but differs from the sketch in Ji and Ziegler (1993, fig. 21.9) showing an unarched narrow platform.

Polygnathus tenellus surinensis new subspecies
Figures 8.1–8.3, 9.12–9.14

Holotype.—P1 element UOPS 570; the specimen illustrated in Figures 9.12–9.14. Repository: Condon Collection, University of Oregon.

Diagnosis.—A polygnathid with a P1 element characterized by numerous fine nodes on platform margins and with one anterior platform margin wider and more forward than the other.

Description.—The P1 element has platform margins bearing numerous fine nodes. One platform margin is wider and extends more forward than the other. The free blade is slightly shorter than the platform. The platform carina has only three or four elongate tubercules. The basal cavity is medium to large and situated close to the anterior of the platform.

Etymology.—After the Mae Surin waterfall, north of the town of Mae Sariang.

Materials.—Holotype plus three paratypes.

Remarks.—The numerous fine nodes on the platform margins extend anteriorly to where the platform meets the blade (Fig. 9.14).

Acknowledgments

Logistic support in 2004–2010 of A. Sardsud of the Thailand Department of Mineral Resources and of P. Lutat of Mahasarakham University is gratefully acknowledged. Some of the photographs in Figure 2 were published previously by Königshof et al. (2012). These were taken in 2010 during a field visit to the Mae Sariang section by the author and P. Königshof, after which photographs were shared. The manuscript was improved by the reviews of D.J. Over and R.T. Becker and the editorial comments of J. Jin, J. Kastigar, B. Hunda, S. Leslie, and H.-D. Sues.

References

Bardashev, I.A., 2009, New Frasnian conodonts of the genus *Palmatolepis* from central Tajikistan: Paleontological Journal, v. 43, p. 300–305.
Becker, R.T., Piecha, M., Gereke, M., and Spellbrink, K., 2016, The Frasnian/Famennian boundary in shelf basin facies north of Diemelsee-Adorf: Münster Fortschritt Geologie und Paläontologie, v. 108, p. 220–231.
Bond, D.P.G., and Grasby, S.E., 2017, On the causes of mass extinctions: Palaeogeography, Palaeoclimatology, Palaeoecology, v. 478, p. 3–29.
Branson, E.R., 1938, Stratigraphy and paleontology of the Lower Mississippian of Missouri. Part 1: University of Missouri Studies, v. 13, 208 p.
Branson, E.R., and Mehl, M.G., 1934, Conodonts of the Grassy Creek Shale of Missouri: University of Missouri Studies, v. 8, p. 171–259.
Branson, E.R., and Mehl, M.G., 1938, The conodont genus *Icriodus* and its stratigraphic distribution: Journal of Paleontology, v. 12, p. 156–166.
Buggisch, W., and Joachimski, M.M., 2006, Carbon isotope stratigraphy of the Devonian of Central and Southern Europe: Palaeogeography, Palaeoclimatology, Palaeoecology, v. 240, p. 68–88.
Burrett, C.F., Carey, S.P., and Wongwanich, T., 1986, A Siluro-Devonian carbonate sequence in northern Thailand: Journal of Southeast Asian Earth Sciences, v. 1, p. 215–220.
Courtillot, V., Kravchinsky, V.A., Quidelleur, X., Renne, P.R., and Gladkochub, D.M., 2010, Preliminary dating of the Viluy traps (Eastern Siberia): Eruption at the time of Late Devonian extinction events?: Earth and Planetary Science Letters, v. 300, p. 239–245.
Dopieralska, J., Belka, Z., Königshof, P., Racki, G., Savage, N., Lutat, P., and Sardsud, A., 2012, Nd isotopic composition of Late Devonian seawater in western Thailand: Geotectonic implications for the origin of the Sibumasu terrane: Gondwana Research, v. 22, p. 1102–1109.
Han, Y.J., 1987, Study on Upper Devonian Frasnian/Famennian boundary in Ma'anshan, Zhongping, Xiangzhou, Guangxi: Bulletin, Chinese Academy Geological Sciences, v. 17, p. 172–194.
Hinde, G.J., 1879, On conodonts from the Chazy and Cincinnati Group of the Cambro-Silurian, and from the Hamilton and Genesee-Shale of the Devonian, in Canada and the United States: Quarterly Journal of the Geological Society of London, v. 35, p. 351–369.
Ji, G., and Ziegler, W., 1993, The Lali Section: An excellent reference section for Upper Devonian in South China: Courier Forschungsinstitut Senckenberg, v. 157, p. 1–183.
Jones, D.S., Martini, A.M., and Kunio, K., 2016, Did volcanism trigger the Late Ordovician mass extinction? Mercury data from South China: Geological Society of America Abstracts with Programs, v. 48, no. 7, doi:10.1130/abs/2016AM-280651.
Kamata, Y., Ueno, K., Hara, H., Ichise, M., Charoentitirat, T., Charusiri, P., and Sardsud, A., 2009, Classification of the Sibumasu and Paleo-Tethys tectonic division in Thailand using chert lithofacies: Island Arc, v. 18, p. 21–31.
Khruscheva, E.N., and Kuz'min, A.V., 1996, New Upper Frasnian conodonts of *Palmatolepis* from the Lyaiol Formation, South Timan: Paleontological Journal, v. 3, p. 90–93.
Kiselev, A.I., Yarmolyuk, V.V., Egorov, K.N., Chernyushov, R.A., and Nikiphorov, A.V., 2006, Middle Paleozoic basite magmatism of the northwest part of the Viluy Rift: Composition, sources, geodynamics: Petrology, v. 6, p. 660–682.
Klapper, G., 1975, *Icriodus symetricus*, Branson and Mehl, 1934, *in* Ziegler, W., ed., Catalogue of Conodonts: Schweizerbart'sche Verlagsbuchhandlung, Stuttgart, v. 2, p. 151–153.
Klapper, G., 2007, Conodont taxonomy and the recognition of the Frasnian/Famennian (Upper Devonian) Stage Boundary: Stratigraphy, v. 4, p. 67–76.
Klapper, G., and Foster, C.T., Jr., 1993, Shape analysis of Frasnian species of the Late Devonian conodont genus *Palmatolepis*: Paleontological Society Memoir 32, 35 p.
Klapper, G., Kuz'min, A.V., and Ovnatanova, N.S., 1996, Upper Devonian conodonts from the Timan-Pechora region, Russia, and correlation with a Frasnian composite standard: Journal of Paleontology, v. 70, p. 131–152.
Königshof, P., Savage, N.M., Lutat, P., Sardsud, A., Dopieralska, J., Belka, Z., and Racki, G., 2012, Late Devonian sedimentary record of the Paleotethys Ocean—The Mae Sariang section, northwest Thailand: Journal of Asian Earth Sciences, v. 52, p. 146–158.

https://doi.org/10.1017/jpa.2018.96 Published online by Cambridge University Press

Metcalfe, I., 2011, Tectonic framework and Phanerozoic evolution of Sundaland: Gondwana Research, v. 19, p. 3–21.
Miller, A.K., and Youngquist, W., 1947, Conodonts from the type section of the Sweetland Creek Shale in Iowa: Journal of Paleontology, v. 21, p. 501–517.
Miller, S.A., 1889, North American Geology and Palaeontology for the Use of Amateurs, Students, and Scientists: Cincinnati, Western Methodist Book Concern, 718 p.
Müller, K.J., 1956, Zur Kenntnis der Conodonten-Fauna des europäischen Devons, 1; Die Gattung *Palmatolepis*: Senckenbergische Naturforschende Gesellschaft Abhandlungen, v. 494, p. 1–70.
Müller, K.J., and Müller, E.M., 1957, Early Upper Devonian (Independence) conodonts from Iowa, Pt. 1: Journal of Paleontology, v. 31, p. 1069–1108.
Ovnatanova, N.S., 1969, Novye verkhnedevonskie conodonty tsentral'nykh rayonov Russkoy Platformy i Timana: Vsesoyuznyy Nauchno-Issledovatel'skiy Geologorazvedochnyy Neftyanoy Institut; Trudy, v. 93, p. 139–141. [in Russian]
Ovnatanova, N.S., 1976, Novye pozdnedevonskie konodonty Russkoy Platformy: Paleontologicheskiy Zhurnal, v. 1976, no. 2, p. 106–115.
Pölsler, P., 1969, Conodonten aus dem Devon der Karnischen Alpen (Findenigkofel, Österreich): Jarbuch der Geologischen Bundesanstalt, v. 112, p. 399–440.
Racki, G., 2005, Toward understanding Late Devonian global events: few answers, many questions, *in* Over, D.J., Morrow, I.R., and Wignall, P.B., eds., Understanding Late Devonian and Permian-Triassic Biotic and Climatic Events: Towards an Integrated Approach: Amsterdam, Elsevier, p. 5–36.
Sandberg, C.A., 1976, Conodont biofacies of Late Devonian *Polygnathus styriacus* Zone in western United States, *in* Barnes, C.R., ed., Conodont paleoecology: Geological Association of Canada, Special Paper 15, p. 171–186.
Sandberg, C.A., and Ziegler, W., 1979, Taxonomy and biofacies of important conodonts of Late Devonian *stryriacus*-Zone, United States and Germany: Geologica et Paleontologica, v. 13, p. 173–212.
Sandberg, C.A., and Ziegler, W., 1992, *Ancyrognathus barbus* n. sp., *in* Sandberg, C.A., Ziegler, W., Dreesen, R., and Butler, J.L., Conodont Biochronology, Biofacies, Taxonomy, and Event Stratigraphy Around Middle Frasnian Lion Mudmound (F2h), Frasnes, Belgium: Courier Forschungsinstitut Senckenberg, v. 150, 87 p.
Sanei, H., Grasby, S.E., and Beauchamp, B., 2012, Latest Permian mercury anomalies: Geology, v. 40, p. 63–66.
Sannemann, D., 1955a, Beitrag zur Untergliederung des Oberdevons nach Conodonten: Neues Jarhbuch für Geologie und Palaontologie, Abhandlungen, v. 100, p. 324–331.
Sannemann, D., 1955b, Oberdevonische Conodonten (to IIa): Senckenbergiana Lethaea, v. 36, p. 123–156.
Savage, N.M., 2013, Late Devonian Conodonts from Northwestern Thailand: Eugene, Bourland Printing, 48 p.
Savage, N.M., and Funai, C.A., 1980, Devonian conodonts of probable early Frasnian age from the Coronados Islands of southeastern Alaska: Journal of Paleontology, v. 54, p. 806–813.
Savage, N.M., Sardsud, A., and Buggisch, W., 2006, Late Devonian conodonts and the global Frasnian-Famennian extinction event, Thong Pha Phum, western Thailand: Paleoworld, v. 15, p. 171–184.
Soboleva, M.A., 2017, [New species of genus *Palmatolepis* (conodonts) from Frasnian deposits of the subpolar and polar Urals]: Syktyvkarskiy Paleontologicheskiy Sbornik, n. 8, (Trudy Instituta Geologii Komi Nauchnogo Tsentra UrO RAN, v. 130), p. 40–50 [in Russian]
Spalletta, C., Perri, M.C., Over, D.J., 2017, Famennian (Upper Devonian) conodont zonation: revised global standard: Bulletin of Geoscience, v. 92, p. 31–57.
Szulczewski, M., 1971, Upper Devonian conodonts, stratigraphy and facial development in the Holy Cross Mountains: Acta Geologica Polonica, v. 21, p. 1–129.
Thibodean, A.M., and Berquist, B.A., 2017, Do mercury isotopes record the signature of massive volcanism in marine sedimentary records?: Geology, v. 45, p. 95–96.
Ulrich, E.O., and Bassler, R.S., 1926, A classification of the toothlike fossils, conodonts, with descriptions of American Devonian and Mississippian species: Proceedings of the U.S. National Museum, v. 68, 63 p.
Wongwanich, T., and Burrett, C.F., 1984, The Lower Palaeozoic of Thailand: Journal of the Geological Society of Thailand, v. 6, p. 21–29.
Ziegler, W., 1958, Conodontenfeinstratigraphische Untersuchungen an der Grenze Mitteldevon/Oberdevon und in der Adorfstufe: Notizblatt des Hessischen Landesamtes für Bodenforschung, v. 87, p. 7–77.
Ziegler, W., 1962, Taxonomie und Phylogenie oberdevonischer Conodonen und ihre stratigraphische Bedeutung: Abhandlungen des Hessischen Landesamtes für Bodenforschung, v. 38, 166 p.
Ziegler, W., and Sandberg, C.A., 1988, *Palmatolepis praetriangularis* n. sp., *in* Sandberg, C.A., Ziegler, W., Dreesen, R., and Butler, J.L., Late Frasnian mass extinction: Conodont event stratigraphy, global changes, and possible causes: Courier Forschungsinstitut Senckenberg, v. 102, p. 298–299.
Ziegler, W., and Sandberg, C.A., 1990, The Late Devonian standard conodont zonation: Courier Forschungsinstitut Senckenberg, v. 121, 115 p.

Accepted: 3 November 2018

https://doi.org/10.1017/jpa.2018.96 Published online by Cambridge University Press